

Article

Gelatin Methacryloyl Hydrogels for the Localized Delivery of Cefazolin

Margaux Vigata ¹, Cathal D. O'Connell ^{2,3}, Silvia Cometta ^{1,4}, Dietmar W. Hutmacher ^{1,4,5,6,7}, Christoph Meinert ^{1,8,*} and Nathalie Bock ^{4,5,9,*}

- ¹ Faculty of Engineering, School of Mechanical, Medical and Process Engineering, Queensland University of Technology, Brisbane, QLD 4000, Australia; margaux.vigata@yahoo.fr (M.V.); silviacatalina.comettaconde@hdr.qut.edu.au (S.C.); dietmar.hutmacher@qut.edu.au (D.W.H.)
- ² Aikenhead Centre for Medical Discovery (ACMD), St Vincent's Hospital Melbourne, Fitzroy, VIC 3065, Australia; cathal.o'connell2@rmit.edu.au
- ³ Discipline of Electrical and Biomedical Engineering, School of Engineering, RMIT University, Melbourne, VIC 3000, Australia
- ⁴ Australian Research Council Training Centre for Multiscale 3D Imaging, Modelling and Manufacturing (M3D Innovation), Queensland University of Technology, Kelvin Grove, QLD 4059, Australia
- ⁵ Faculty of Health, School of Biomedical Sciences, Queensland University of Technology, Brisbane, QLD 4000, Australia
- ⁶ Australian Research Council Industrial Transformation Training Centre in Additive Biomanufacturing, Queensland University of Technology, Brisbane, QLD 4059, Australia
- ⁷ Australian Research Council Training Centre for Cell and Tissue Engineering Technologies, Queensland University of Technology, Brisbane, QLD 4059, Australia
- ⁸ Herston Biofabrication Institute, Metro North Hospital and Health Services, Herston, QLD 4006, Australia
- ⁹ Translational Research Institute, Woolloongabba, QLD 4102, Australia
- * Correspondence: christoph.meinert@qut.edu.au (C.M.); n.bock@qut.edu.au (N.B.); Tel.: +61-(0)-450-177-179 (C.M.); +61-(0)7-3443-7343 (N.B.)



Citation: Vigata, M.; O'Connell, C.D.; Cometta, S.; Hutmacher, D.W.; Meinert, C.; Bock, N. Gelatin Methacryloyl Hydrogels for the Localized Delivery of Cefazolin. *Polymers* **2021**, *13*, 3960. <https://doi.org/10.3390/polym13223960>

Academic Editor: Kumkum Ahmed

Received: 28 October 2021

Accepted: 12 November 2021

Published: 16 November 2021

Publisher's Note: MDPI stays neutral with regard to jurisdictional claims in published maps and institutional affiliations.



Copyright: © 2021 by the authors. Licensee MDPI, Basel, Switzerland. This article is an open access article distributed under the terms and conditions of the Creative Commons Attribution (CC BY) license (<https://creativecommons.org/licenses/by/4.0/>).

Abstract: The tuneability of hydrogels renders them promising candidates for local drug delivery to prevent and treat local surgical site infection (SSI) while avoiding the systemic side-effects of intravenous antibiotic injections. Here, we present a newly developed gelatin methacryloyl (GelMA)-based hydrogel drug delivery system (GelMA-DDS) to locally deliver the broad-spectrum antibiotic cefazolin for SSI prophylaxis and treatment. Antibiotic doses from 3 µg to 90 µg were loaded in photocrosslinked GelMA hydrogel discs with 5 to 15% *w/v* polymer concentration and drug encapsulation efficiencies, mechanical properties, crosslinking and release kinetics, as well as bacterial growth inhibition were assessed. Our results demonstrate that all GelMA groups supported excellent drug encapsulation efficiencies of up to 99%. Mechanical properties of the GelMA-DDS were highly tuneable and unaffected by the loading of small to medium doses of cefazolin. The diffusive and the proteolytic *in vitro* drug delivery of all investigated cefazolin doses was characterized by a burst release, and the delivered cefazolin amount was directly proportional to the encapsulated dose. Accelerated enzymatic degradation of the GelMA-DDS followed zero-order kinetics and was dependent on both the cefazolin dose and GelMA concentration (3–13 h). Finally, we demonstrate that cefazolin delivered from GelMA induced a dose-dependent antibacterial efficacy against *S. aureus*, in both a broth and a diffusive assay. The cefazolin-loaded GelMA-DDS presented here provides a highly tuneable and easy-to-use local delivery system for the prophylaxis and treatment of SSI.

Keywords: gelatin methacryloyl; cefazolin; localized antibiotic therapy; drug delivery; surgery site infection

1. Introduction

Medical procedures present an inherent risk of surgical site infection (SSI) [1]. Hospital-acquired infections, also known as nosocomial infections, are the most frequent SSI reported.

SSI represents 15–20% of all nosocomial infections and, hence, have a significant economic and human impact [2,3]. The most common pathogens implicated in SSI are *S. aureus*, *S. epidermidis*, and Coagulase-negative *Staphylococci*, but an increasing number of SSI reported are attributed to methicillin-resistant *S. aureus* (MRSA) [1,3,4].

Cefazolin is amongst the most commonly used antibiotic agents to combat and prevent SSI [3,5–7]. It is a bactericidal first-generation beta-lactam antibiotic that binds to penicillin-binding proteins, which are the catalyzer for peptidoglycan synthesis, and thus disrupts the bacteria wall formation, causing the bacteria to lyse [8]. Cefazolin is often used perioperatively due to its effectiveness against a wide range of gram positive (*Staphylococci* and *Streptococci*) and gram-negative bacteria (*Escherichia coli* or *Proteus mirabilis*) [3,5,6]. Despite its common usage, systemic administration of cefazolin can lead to severe side effects ranging from allergic reactions to encephalopathy or epilepsy [9]. Additionally, a growing concern is the potential for acquired antibiotic resistance resulting from systemic administration of cefazolin [10–13].

Controlled local delivery of drugs has been proposed as an approach to overcome the risks associated with antibiotic overuse, since drugs delivered locally require significantly lower doses compared to systemic approaches [14]. Local drug delivery systems (DDS) can effectively control drug bioavailability to target cells and tissue over time and space to leverage beneficial outcomes of therapeutics enhancing efficacy and reducing toxicity and required dosage [15]. Various DDS classes have been explored in scientific literature, including membranes [16], nanoparticles [17], liposomes [18], and hydrogels [15]. Hydrogels are a particularly interesting material class for DDS and have been extensively used in many branches of medicine and tissue engineering. Hydrogels are composed of crosslinked polymer networks that hold large amounts of water, often ranging from 70 to 99% of wet weight. This high-water content provides similarities to native tissue and excellent biocompatibility, as well as the ability to easily retain hydrophilic drugs. Furthermore, because of their formation in aqueous conditions, risks associated with drug aggregation and denaturation are minimized [15]. Hydrogels provide excellent tuneability of their physical properties that enable precise matching of soft tissue properties in the human body [19]. On a nanometre scale, crosslinked hydrogel networks provide tuneable porosity, referred to as the mesh size, which governs and controls drug diffusion within and from hydrogel-based DDS. Therefore, the modularity, intrinsic properties, and tuneability of hydrogels enable precise tailoring of drug release in time and space, rendering this class of materials promising for clinical local drug delivery applications [15].

In this work, we developed a hydrogel DDS based on gelatin methacryloyl (GelMA) for the local release of cefazolin. To retain simplicity and clinical relevance, the antibiotic was loaded with the GelMA hydrogel precursor solution before photocrosslinking. GelMA is a semi-synthetic hydrogel that retains the advantages of polymers of natural origin, i.e., biocompatibility, low immunogenicity, and biodegradability, owing to its natural metalloprotease-cleavable motifs. The functionalization of gelatin by the addition of methacryloyl groups enables enhanced control over the physicochemical properties of the hydrogel [20]. Additionally, GelMA is a well-described biomaterial to which physical properties can be tailored based on crosslinking conditions [21]. The stiffness of the hydrogel is directly proportional to the mesh size of the hydrogel matrix, which, in turn, is used to tune the release of therapeutic molecules [22]. Li et al. described the release mechanisms of drugs from hydrogel polymers: diffusion through the matrix, swelling, or degradation. Drugs smaller than the hydrogel mesh size will follow a fast diffusion, while drugs of similar or larger size will be slowed down and/or retained. In the latter case, the therapeutic molecule release can follow other mechanisms involving hydrogel deformation, swelling, or degradation [15].

We hypothesized that different GelMA concentrations would allow the ability to tailor physical properties such as matrix stiffness, porosity, water content, permeability, and diffusive properties, which have previously been shown to have an effect on the antibiotic release kinetics in other hydrogel systems [22,23]. We first evaluated the in vitro release

of cefazolin in phosphate-buffered saline (PBS) and following collagenase degradation. The release kinetics characterization was completed by assessing the hydrogels' swelling properties and related mesh size. Then, we characterized the mechanical properties of the GelMA-DDS loaded with several cefazolin doses, as well as the impact of cefazolin on the gelation time and polymerization kinetics. Finally, we studied the in vitro antibacterial efficacy of the cefazolin-loaded GelMA-DDS in a zone of inhibition assay and a broth assay of the bacterium *S. aureus*.

2. Material and Methods

2.1. Drug Encapsulation and GelMA Crosslinking

Gelatin methacryloyl (GelMA; porcine skin, type A, ~80% degree of functionalization) was provided by Gelomics (Gelomics, Brisbane, Australia). GelMA-drug delivery system (DDS) samples for in vitro assays were manufactured using a mold casting technique. Custom polytetrafluoroethylene (PTFE) molds were used to make disc-shaped samples measuring 5 mm diameter and 1.8 mm height and ~35 μ L of volume. Hydrogel discs based on 5%, 10%, or 15% GelMA containing 0 μ g, 3 μ g, 15 μ g, 30 μ g, or 90 μ g cefazolin (Sigma-Aldrich, St Louis, MO, USA) (Table 1), respectively, were prepared by ultraviolet (UV) crosslinking at 365 nm for 30 min (intensity of ~2.6 mW/cm² in a CL-1000 crosslinker; UVP, Upland, CA, USA) in the presence of and 0.05 % *w/v* Irgacure 2959 (1-[4-(2-hydroxyethoxy)-phenyl]-2-hydroxy-2-methyl-1-propanone, BASF, Ludwigshafen, RLP, Germany). Hydrogel samples were stored at 4 °C until use.

Table 1. Experimental groups denomination and composition.

Group Denomination	GelMA Concentration (%)	Cefazolin Dose (μ g)
5% GelMA	5	0
5% GelMA–30 μ g	5	30
10% GelMA	10	0
10% GelMA–3 μ g	10	3
10% GelMA–15 μ g	10	15
10% GelMA–30 μ g	10	30
10% GelMA–90 μ g	10	90
15% GelMA	15	0
15% GelMA–30 μ g	15	30

2.2. Release Study

Drug release studies were carried out in PBS at pH 7.4, 37 °C, and under 75 rpm agitation in an orbital incubator. Each hydrogel sample (*n* = 6) was immersed in 0.5 mL of PBS in low protein binding tubes (Eppendorf Protein LoBind Tubes, Hamburg, Germany), and the entire volume was sampled and refreshed at the different timepoints.

2.2.1. Drug Detection

Cefazolin quantification was performed using ultra-high-performance liquid chromatography with tandem mass spectrometry (UHPLC-MS-MS) using a Nexera X2 UHPLC system coupled to a triple quadrupole mass spectrometer Shimadzu LCMS-8050 (Shimadzu, Kyoto, Japan). All samples were filtered using 0.2 μ m pore size syringe filters. The separation flow rate was of 0.3 mL/min using a Kinetex[®] 2.6 μ m EVO C18 100 Å LC column 100 \times 2.1 mm (Phenomenex, Tokyo, Japan). The mobile phase A was water with 0.1% formic acid, while the mobile phase B consisted of 0.1% formic acid in acetonitrile. Samples were placed in the autosampler, in which temperature was set at 5 °C, and the injection volume was 1 μ L. Cefazolin ionization was executed by a positive-ion electrospray with a nebulizing gas flow of 3 L/min, the heating gas flow of 10 L/min, drying gas flow

of 10 L/min, interface temperature of 300 °C, desolvation line (DL) temperature of 250 °C, and heat block temperature of 400 °C.

2.2.2. Encapsulation Efficiency

Drug-loaded hydrogel samples ($n = 6$) were degraded overnight at 37 °C and 300 rpm on a Thermomixer Compact (Eppendorf, Hamburg, Germany) in 0.5 mL Hank's Balanced Salt Solution (Gibco™ HBSS, calcium, magnesium, no phenol red, Thermo Fischer Scientific, Waltham, MA, USA) containing 28 units/mL collagenase II (Gibco™ Collagenase, Type II powder, Thermo Fischer Scientific, Waltham, MA, USA). Cefazolin drug quantification was performed with HPLC-MS-MS as outlined above. Supplementary Figure S1 shows an offset in the cefazolin detection used to create standard curves between the drug detected in a PBS solution versus a collagenase-HBSS solution. The detection of cefazolin in collagenase and HBSS solution was, on average, 13.37% lower. Consequently, the encapsulation efficiencies measured were corrected by a factor of 1.1337.

2.2.3. Degradation Characterization

To simulate in vivo environments and investigate the release of cefazolin in response to proteolytic degradation, accelerated enzymatic degradation of the GelMA hydrogels was performed in vitro using collagenase. Hydrogel samples ($n = 4$) were digested at 37 °C, at 300 rpm, in 0.5 mL of 28 units/mL collagenase (Gibco™ Collagenase, Type II powder, Thermo Fischer Scientific, Waltham, MA, USA) in Hank's Balanced Salt Solution (Gibco™ HBSS, calcium, magnesium, no phenol red, Thermo Fischer Scientific, Waltham, MA, USA). Every two hours, the hydrogels were weighed, and the collagenase solution was refreshed. The degradation rate was calculated using the ratio of the digested mass over the original mass.

2.2.4. Release via Degradation

Samples ($n = 3$) were digested in 0.5 mL of 28 units/mL collagenase II (Gibco™ Collagenase, Type II powder, Thermo Fischer Scientific, Waltham, MA, USA) at 37 °C and 300 rpm on a thermomixer compact (Eppendorf, Hamburg, Germany). Every two hours, the digestion media was sampled for drug detection and refreshed. Drug detection was carried out using HPLC-MS-MS.

2.2.5. Equilibrium Mass Swelling Ratio and Mesh Size Calculation Equilibrium Mass Swelling Ratio

For this study, two control groups were added: 5% GelMA and 15% GelMA. Samples ($n = 5-7$) were weighed after seven-day swelling to equilibrium in PBS at 37 °C, and then again after freeze-drying. The equilibrium mass swelling ratio (Q_m) was calculated according to the following equation:

$$Q_m = \frac{(m_{wet} - m_{lyophilized})}{m_{lyophilized}} \quad (1)$$

where m_{Wet} is the wet mass after swelling and $m_{lyophilized}$ is the mass after lyophilization of the hydrogel samples.

2.2.6. Mesh Size Calculation

The mesh size ξ of the GelMA hydrogels was determined using the mass swelling ratio, and the inherent characteristics such as the molecular weight between crosslinks, the molecular weight of the repeating unit, the bond length, and the equilibrium polymer volume fraction (v_{2s}), of gelatin and GelMA hydrogels [24,25] in Equation (2).

Mesh size was calculated using the molecular weight of the repeating unit M_r (averaged molecular weight of the amino acid composition, $M_r = 91.19$ g/mol) [26], the amino acid bond length $l = 4.28$ Å [27], the Flory's characteristic ratio C_n for GelMA was

taken as 8.8785 [26], and the molecular weight between crosslinks M_c was calculated using Equation (5).

$$\xi = v_{2s}^{-\frac{1}{3}} \times l \left(2 \frac{M_c}{M_r} C_n \right)^{\frac{1}{2}} \quad (2)$$

The relaxed volumetric swelling Q_{vr} and the equilibrium volumetric swelling Q_v were obtained by converting the respective relaxed mass swelling ratio Q_{mr} and the equilibrium mass swelling ratio Q_m using the gelatin density as polymer density ($\rho_p = 1.35 \text{ g/cm}^3$) [28–30] and the PBS density as solvent density ($\rho_s = 1.014 \text{ g/cm}^3$) [31] in Equation (3). The relaxed mass swelling ratio Q_{mr} and the equilibrium mass swelling ratio Q_m were obtained with Equation (1) using the wet weight just after crosslinking and after reaching equilibrium swelling, respectively.

$$Q_{v(r)} = 1 + \frac{\rho_p}{\rho_s} (Q_{m(r)} - 1) \quad (3)$$

Then the relaxed polymer volume fraction v_{2r} and the equilibrium polymer volume fraction v_{2s} were calculated using Equation (4).

$$v = \frac{1}{Q_v} \quad (4)$$

Finally, the molecular weight between crosslinks M_c (g/mol) was estimated using the Flory-Rhener Equation (5) used for polymers crosslinked in solvents [24,32,33]. The polymer properties such as the specific volume of the polymer \bar{v} taken as 0.7407 mL/g [26], the molar volume of the solvent V_1 was 18.01 mL/mol for water [26], the polymer-solvent interaction X_1 , which is known as the Flory's Chi parameter, was 0.497 [34], and the number average molecular weight before crosslinks M_n (63,565.35 g/mol) [35].

$$\frac{1}{M_c} = \frac{2}{M_n} - \frac{\bar{v}}{V_1} \frac{[\ln(1 - v_{2s}) + v_{2s} + X_1 v_{2s}^2]}{v_{2r} \left[\left(\frac{v_{2s}}{v_{2r}} \right)^{\frac{1}{3}} - \frac{1}{2} \left(\frac{v_{2s}}{v_{2r}} \right) \right]} \quad (5)$$

2.3. Mechanical and Physical Properties

2.3.1. Effective Mass Swelling

Samples ($n = 8$) were weighed immediately after crosslinking and then again after overnight swelling in PBS at 37 °C. The mass difference was expressed as a percentage to assess the effective mass swelling of the hydrogel-DDS:

$$\text{Effective swelling (\%)} = \frac{(m_{\text{Wet}} - m_{\text{initial}})}{m_{\text{initial}}} \times 100\% \quad (6)$$

where m_{Wet} is the wet mass after swelling and m_{initial} is the mass just after crosslinking and before swelling.

2.3.2. Mechanical Compression Test

Compressive moduli, failure strain, failure stress, and toughness of GelMA-DDS samples ($n = 8$) were investigated in unconfined compression tests using an Instron 5848 microtester with a 500 N load cell (Instron, Melbourne, VIC, Australia). Before testing, samples were immersed overnight in PBS at 37 °C to facilitate swelling to equilibrium. During the test, samples were also immersed in PBS at 37 °C, and a non-porous aluminum indenter was used to apply compression with a displacement rate of 0.01 mm/s on the hydrogel samples. The slope of the strain-stress curve, from 10% to 15% strain, was used to determine the Young's compressive modulus [20]. The maxima of the stress-strain curve before the hydrogel sample cracking (sudden drop in the stress-strain curve) determined the failure stress and strain. The toughness was defined as the area under the stress-strain

curve from 0% strain until failure. A previously published automated algorithm was used for mechanical testing data analysis [36].

2.3.3. Photorheology

Samples ($n = 5$) of the hydrogel precursor solution containing 0.05% Irgacure with and without cefazolin were analyzed on a rheometer (Physica MCR 302 Rheometer, Anton Paar, Graz, Austria), using a cone-plate configuration (15 mm disk, 1° cone angle, and a 31 μm truncation at the apex), at room temperature, (23°C). Measurements were performed under oscillatory conditions at 0.5% strain and a frequency of 10 rad/s. The samples were photocrosslinked in situ with the aid of a UV light source (Omnicure S1000, Alpha UV Systems, Pymble, Australia) placed under a quartz crystal sample holder. An intensity of 365 nm was calibrated at $3\text{ mW}/\text{cm}^2$ using a radiometer (Omnicure R2000, Alpha UV Systems, Pymble, Australia). For a more comprehensive study, two groups were added: 5% GelMA-90 μg of cefazolin and 15% GelMA 90 μg of cefazolin, as well as their respective control groups: 5% GelMA and 15% GelMA.

2.4. Bacterial Culture

2.4.1. Maintenance

Staphylococcus aureus (*S. aureus*) ATCC29213 was used for the different antibacterial assays. Lysogeny Broth (LB) agar plates were used for the culture.

2.4.2. Zone of Inhibition Assay

A diffusion assay was performed using Mueller-Hinton (MH) agar-containing Petri dishes. A 0.5 McFarland standard solution [37] was prepared by suspending *S. aureus* colonies in MH broth and obtaining an optical density at 600 nm (OD_{600}) between 0.08 and 0.1. To each MH Petrie dish, 30 μL of the solution was added and spread homogeneously. GelMA without loaded cefazolin and antimicrobial susceptibility test discs containing 30 μg of cefazolin (Oxoid, Thermo Fischer Scientific, MA, USA) were used as negative and positive controls, respectively. Plates were incubated overnight at 37°C , plates were imaged, and the zones of inhibition were measured using Fiji ImageJ software. The experiment was performed three times with $n = 6$ each time.

2.4.3. Broth Inhibition Assay

The minimum inhibitory concentration (MIC) of cefazolin for *S. aureus* ATCC29213 after 24 h was between 1.3 and 11.2 $\mu\text{g}/\text{mL}$ for broth inoculum between 5×10^5 CFU/mL and 5×10^7 CFU/mL [38]. Therefore, we used an inoculum broth in the same range (5×10^6 CFU/mL). We modified the assay, which usually lasts 24 h, to study the antibacterial efficacy of the cefazolin-loaded GelMA-DDS over a longer time-period by refreshing the bacteria broth every day for four days. The expectation was that all cefazolin doses encapsulated in the GelMA-DDS would successfully inhibit the bacteria growth for at least the first day of culture.

A 0.5 McFarland standard solution [37] was prepared in MH broth (5×10^8 CFU/mL), and diluted to obtain a broth inoculum at 5×10^6 CFU/mL. GelMA-DDS samples, a positive control, i.e., antimicrobial susceptibility test disc containing 30 μg of cefazolin (Oxoid, Thermo Fisher Scientific, MA, USA) and a free dose of 30 μg of cefazolin, as well as negative control (GelMA without cefazolin), were placed individually in the wells of a 48-well plate. The assay was launched upon the addition of 0.5 mL of prepared bacteria inoculum solution per well. At each timepoint (day 1, day 2, day 3, and day 4), the turbidity was measured using OD_{600} , and a new bacteria broth solution was prepared to replace the 0.5 mL of media in each well completely. The experiment was performed three times with $n = 6$ each time.

2.5. Statistical Analysis

Probabilities of $p \leq 0.05$ were considered a significant difference. Statistical analysis was performed by analysis of variance (ANOVA). The significance of mean differences between groups was calculated using a general linear model (univariate analysis) using IBM SPSS Statistics 23 (IBM Corp., Armonk, NY, USA).

3. Results and Discussion

3.1. Drug Release

In the first part of the study, we evaluated the drug encapsulation efficiencies and characterised in vitro drug release in PBS to provide diffusive release kinetics in physiological conditions. Furthermore, the in vitro drug release via accelerated enzymatic degradation was evaluated because metalloproteases degrade GelMA hydrogels in the body [39]. The equilibrium swelling and the GelMA-DDS mesh size were determined to complete the drug release characterization because the mesh size is the primary physical parameter able to control drug diffusion [15]. The second part focused on the impact of drug loading on the mechanical and swelling properties of the GelMA-DDS because these physical properties are main drivers of drug diffusion [22]. To further investigate the effect of drug loading on the crosslinking reaction of the GelMA-DDS, in situ photorheology experiments were conducted. Finally, in the third and last section, we evaluated the antibacterial efficacy of the cefazolin-loaded GelMA-DDS in a zone of inhibition and a broth assay against the model bacteria *S. aureus*.

3.1.1. Encapsulation Efficiency

We first investigated the encapsulation efficiencies (EE) of cefazolin, defined as the percentage of cefazolin successfully encapsulated in our GelMA-DDS compared to the initial theoretical amount of drug loaded (Figure 1). In our study, EEs of cefazolin in the GelMA-DDS based on 10% GelMA were $\geq 84\%$ for all drug doses, except for 3 μg cefazolin which averaged at 64.7%. The EE of 30 μg cefazolin was similar between 5%, 10% and 15% GelMA, suggesting that the macromolecule concentration did not influence this parameter.

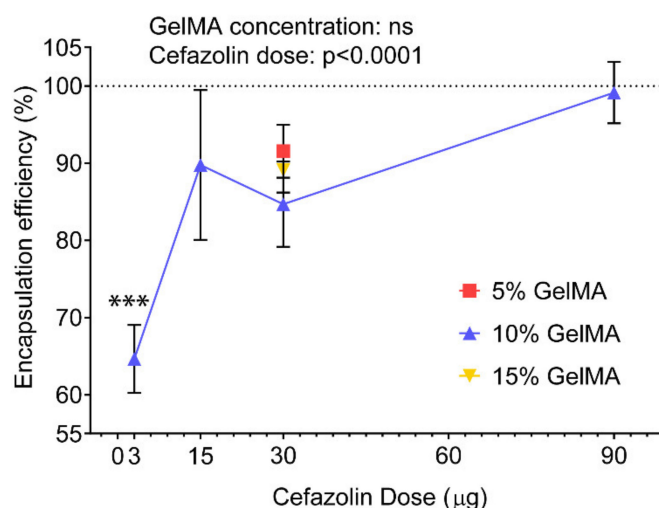


Figure 1. Encapsulation efficiencies of cefazolin in 5%, 10%, and 15% gelatin methacryloyl (GelMA) hydrogels prepared by blend-loading. Results are shown as mean \pm standard deviation, $n = 6$. *** $p < 0.001$ compared to all other groups.

The EEs obtained here were significantly higher compared to work previously published by Shah et al., who obtained limited loading efficiency for cefazolin in poly(DL-lactic-co-glycolic acid) (PLGA) nanoparticles [40]. In their study, Shah et al. attributed the poor EE to a combination of charge incompatibility and polymer phase concentration

between the negatively charged cefazolin and poly(DL-lactic-co-glycolic acid) (PLGA) microparticles, which are relatively hydrophobic [40]. The increased EEs obtained using GelMA as a drug carrier suggest that hydrogels present a more suitable environment for cefazolin encapsulation, a finding that is in accordance with other studies [41–43].

3.1.2. Diffusive Release

Different doses of cefazolin (3 µg, 15 µg, 30 µg, and 90 µg) were loaded in 10% GelMA hydrogels to evaluate the impact of the dose parameter on the diffusive drug release in PBS. To evaluate the effects of GelMA concentrations on antibiotic release, different concentrations of GelMA (5%, 10%, and 15%) were used to encapsulate the same dose of cefazolin (30 µg). Other studies have demonstrated that increasing the GelMA concentration decreases hydrogel mesh size [26,44], leading to higher stiffness [22] and lower permeability [22]. Notably, such tailoring of the GelMA crosslinking conditions was used to control the release of the anticancer drug doxorubicin, which is of similar molecular weight to cefazolin [45,46]. Different crosslinking times were applied to photo-cure the doxorubicin-loaded GelMA-DDS, thereby tailoring the GelMA-DDS mesh size and, ultimately, the doxorubicin release was a more sustained release with the stiffer GelMA-DDS groups [23].

The release profiles of cefazolin at different doses and concentrations all displayed a burst release via diffusion (Figure 2A–D). Overall, around 70% to 92% of the drug cargo was released within one hour of incubation in PBS. In all cases, the total drug cargo was released within the first 12 h of the assay, suggesting that the cefazolin molecules diffuse out of the hydrogel matrix with ease. The GelMA concentration did not impact the release kinetics, whereas the cefazolin dose was a significant parameter that allowed us to tailor drug delivery (Figure 2C,D). The corresponding release rates (Figure 2E,F) displayed a maximum release rate between 0 and 1 h, which decreased following an exponential decay. Analysis of release rates confirmed burst release and its dependency on the cefazolin dose, but not on the GelMA concentration. The maximum cefazolin release rates increased from 1.42 µg/h to 74 µg/h in a dose-dependent manner, demonstrating that release could be tailored by amount of cefazolin loaded in the GelMA-DDS (Figure 2G and Supplementary Figure S2).

Contrary to Luo et al.'s study, our results did not show control over drug release kinetics when modifying the crosslinking conditions of the GelMA-DDS. This is likely explained by the nature of the drug used in this study, doxorubicin, a highly hydrophobic molecule [47], versus cefazolin that presents high hydrophilicity. It is cefazolin's high water solubility that favors its rapid diffusion from the hydrogel into the aqueous release media [45]. Our results therefore suggest that not only the physical tailoring of the hydrogel-DDS should be considered but also the drug hydrophilicity, which dictates its stability and affinity for the hydrogel polymer and released media [48].

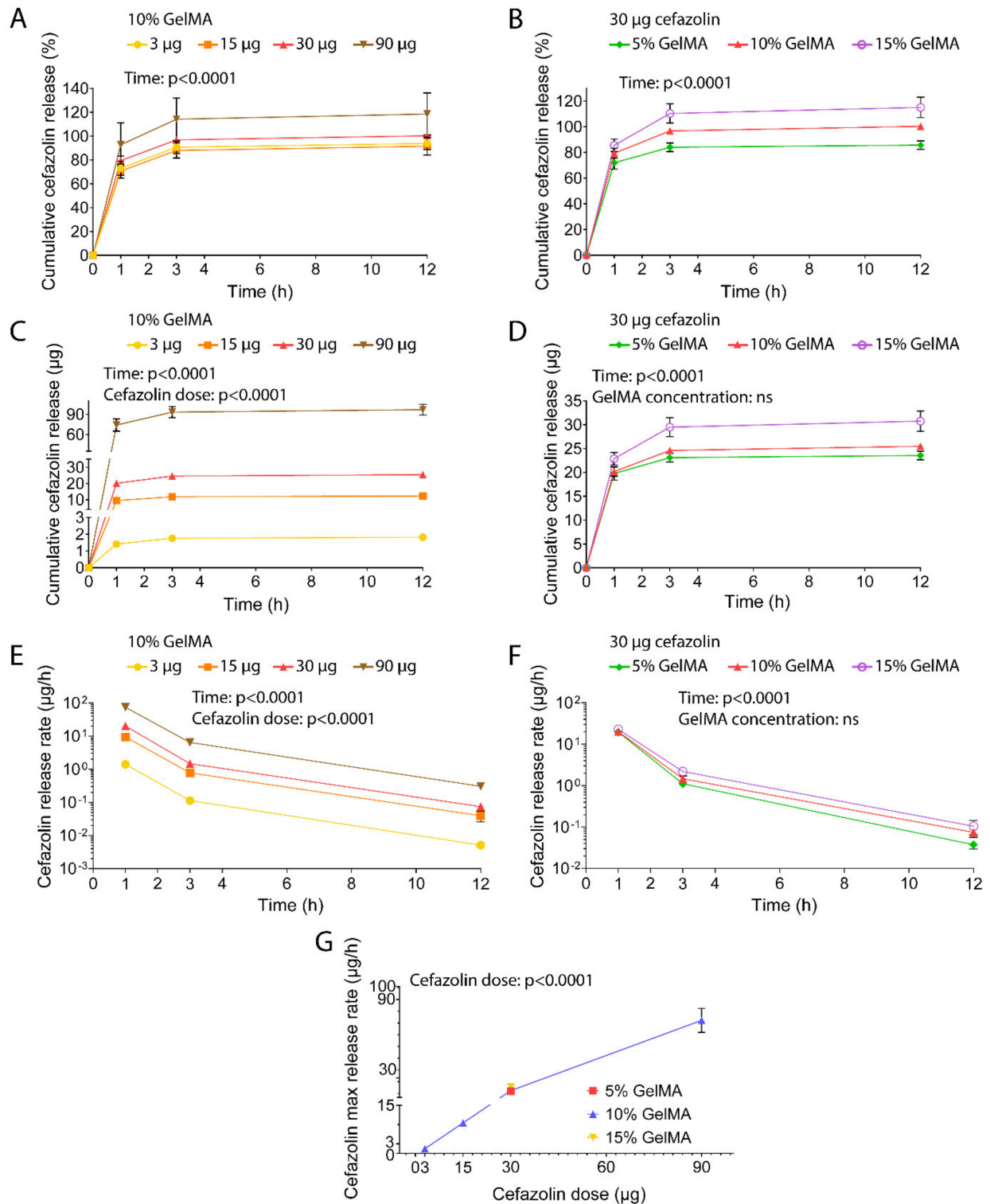


Figure 2. In vitro release of cefazolin in phosphate-buffered saline at pH 7.4, under 75 rpm agitation at 37 °C. (A) Cefazolin cumulative release for 3 μg , 15 μg , 30 μg , and 90 μg from 10% GelMA expressed as percentage of the encapsulation efficiency. (B) Cefazolin cumulative release for 30 μg from 5%, 10%, and 15% GelMA expressed as percentage of the encapsulation efficiency. (C) Cefazolin cumulative release for 3 μg , 15 μg , 30 μg , and 90 μg from 10% GelMA expressed in μg . (D) Cefazolin cumulative release for 30 μg from 5%, 10%, and 15% GelMA expressed in μg . (E) Cefazolin release rate per hour for 3 μg , 15 μg , 30 μg , and 90 μg from 10% GelMA expressed in $\mu\text{g}/\text{h}$. (F) Cefazolin release rate per hour for 30 μg from 5%, 10%, and 15% GelMA expressed in $\mu\text{g}/\text{h}$. (G) Cefazolin maximum release rate at 1 h expressed in $\mu\text{g}/\text{h}$. Data are shown as mean \pm standard deviation. The experiment was performed once with $n = 6$ technical replicates.

3.1.3. Release via Enzymatic Degradation

GelMA hydrogels harbor degradation sites susceptible to metalloproteases such as collagenases and upon implantation undergo proteolytic degradation [39,49]. Thus, the cefazolin release was quantified as the hydrogels were degraded in vitro by collagenase (Figure 3) to simulate in vivo conditions.

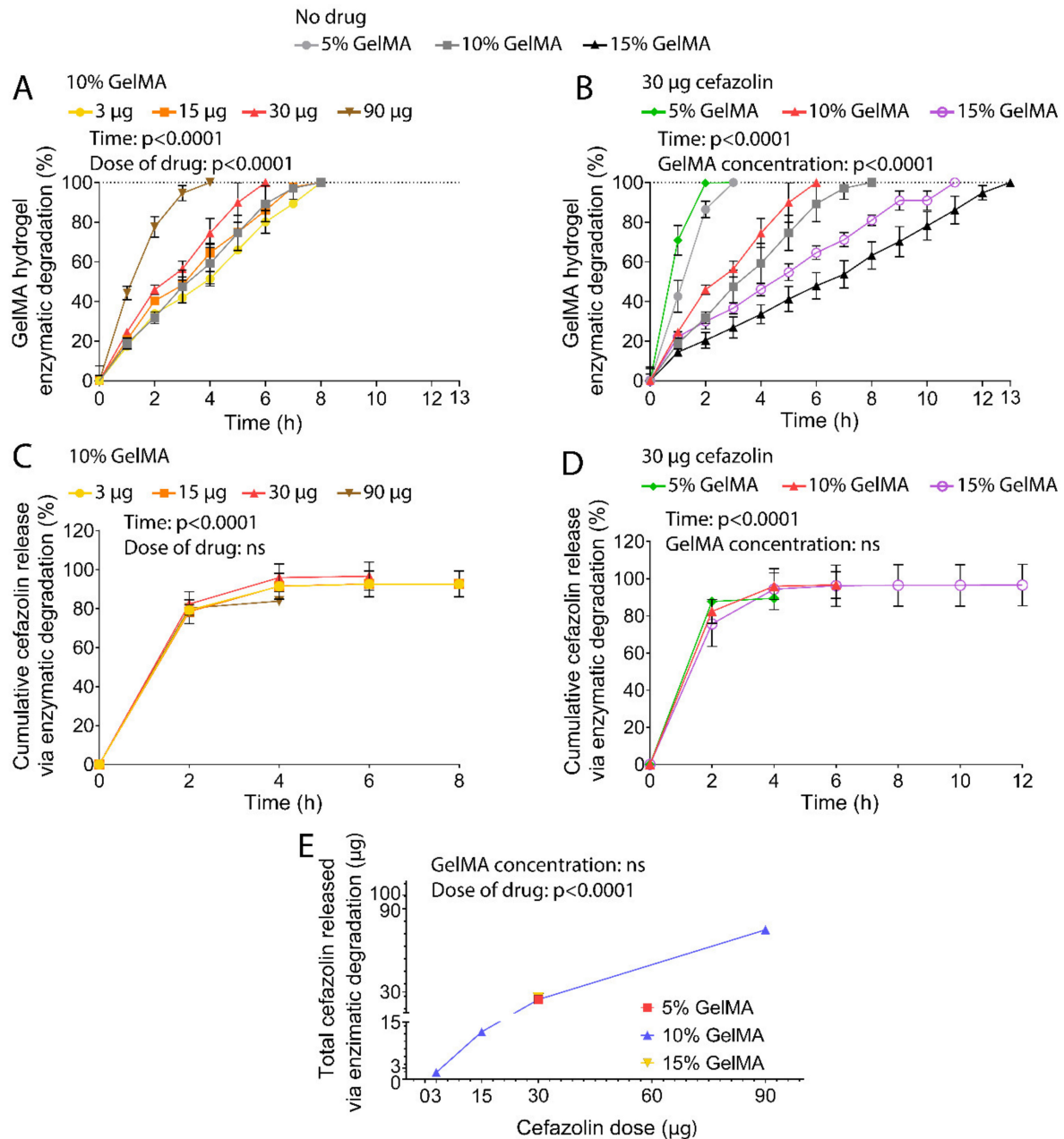


Figure 3. In vitro proteolytic release of cefazolin via collagenase II degradation of GelMA hydrogels at 28 units/mL under 300 rpm agitation at 37 °C. (A) Hydrogel degradation defined as mass loss normalized to initial mass for 5%, 10%, and 15% GelMA and 3 μg , 15 μg , 30 μg , and 90 μg of Cefazolin in 10% GelMA. (B) Hydrogel degradation in mass loss normalized to initial mass for 5%, 10%, and 15% GelMA and 30 μg of Cefazolin in 5% and 15% GelMA. Data are shown as mean \pm standard deviation. The experiment was performed once with $n = 4$. Cumulative release as the percentage of the respective encapsulation efficiencies from GelMA hydrogels. (C) Cumulative release of Cefazolin 3 μg , 15 μg , 30 μg , and 90 μg from 10% GelMA. (D) Cumulative release of Cefazolin 30 μg from 5%, 10%, and 15% GelMA. (E) Total cefazolin released via enzymatic degradation in μg . Data are shown as mean \pm standard deviation. Standard deviations that are not distinguishable are too small thus occluded by the symbols. The experiment was performed once with $n = 3$.

In line with our previous work [50], incubation times required to achieve full hydrogel degradation were inversely proportional to the GelMA concentration (Figure 3A,B). Gels with 5% GelMA concentration degraded in 3 h, while 10% GelMA hydrogels degraded within 8 h, and 15% GelMA hydrogels took 13 h to degrade fully. Cefazolin loading with doses ranging from 3–30 μg did not significantly alter degradation profiles of GelMA-DDS based on 10% macromere concentration. However, degradation of 10% GelMA-DDS with 90 μg cefazolin occurred significantly faster than antibiotic-free control groups, suggesting that encapsulation of high cefazolin doses may lead to structural changes in the macromolecular phase, leading to enhanced permeability. In theory, increased hydrogels porosity and permeability can be related to decreased crosslinking density [22,39,51], which would, in turn, improve the access of the enzyme to the hydrogel scaffold, thereby increasing the proteolytic degradation rate [52,53]. This is further supported by the observation of the degradation curve profiles which were approximately linear for higher concentrations of GelMA (10% and 15%), both without loaded cefazolin and with doses ranging between 3 and 30 μg , suggesting a zero-order degradation rate characteristic of surface erosion. Low concentration hydrogels (5% GelMA) and 10% GelMA-DDS with 90 μg cefazolin, on the other hand, displayed more sigmoid-like profiles characteristic of bulk erosion. Together, these observations suggest that hydrogel mesh size, which is inversely proportional to the hydrogel concentration, was reduced by the encapsulation of high cefazolin doses in 10% GelMA, which in turn led to increased enzyme diffusion into the hydrogel favouring bulk erosion of the macromolecular phase [54–57].

Accelerated proteolytic release of cefazolin presented a burst release in the first two hours. After two hours of release, around 78% to 87% of the drug cargo was released, and complete release was achieved after 4 h for all groups tested (Figure 3C,D). The GelMA concentration did not significantly impact the release kinetics. Yet, similar to the diffusive release, the cefazolin dose encapsulated in the GelMA-DDS dictated the total amount released (Figure 3E). Furthermore, the drug cargo's full release was achieved before the total degradation of 10% and 15% GelMA hydrogels, indicating that the drug diffused out from the hydrogels faster than degradation occurred.

3.1.4. Mesh Size

The hydrogel mesh size ξ , defined as the distance between consecutive chain crosslinks [58], is a primary characteristic of hydrogel systems and dictates their degradation rate [39], swelling properties [58,59], and the diffusive release of molecules from hydrogel-DDS [15]. Thus, the mesh size is an essential factor in predicting drug release behavior. However, this parameter is difficult to determine experimentally [60] and, consequently, is commonly estimated mathematically based on the equilibrium swelling ratio and the Flory-Rehner equation [24,26,32,58].

The equilibrium swelling ratio of the GelMA-DDS and the respective control groups presented in Figure 4A displayed a significant effect of the GelMA concentration. The GelMA concentration was inversely correlated with the swelling ratio which decreased from around 11.4 to 4.7 for gels with 5% to 15% macromere concentration. There was also a significant effect of the cefazolin dose loaded in GelMA. The highest dose of cefazolin (90 μg) in 10% GelMA presented an equilibrium swelling ratio of 9, which is significantly higher than the control group (10% GelMA) and closer to the value of the 5% GelMA hydrogels. This may be indicative of a lower crosslinking density that would also translate into a lower hydrogel stiffness.

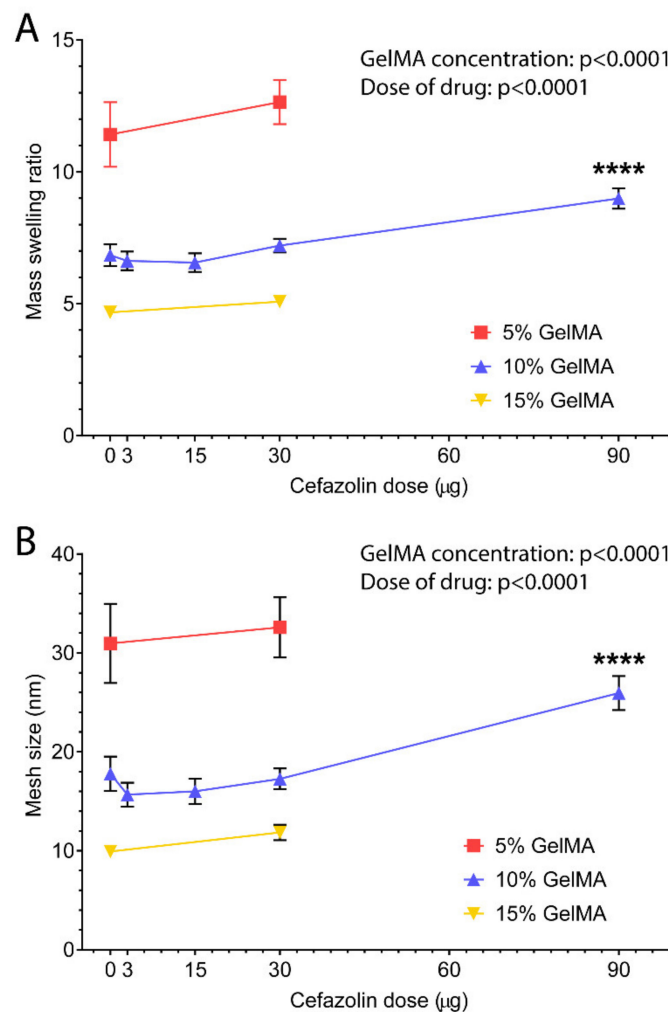


Figure 4. Equilibrium swelling ratio and mesh size of GelMA. GelMA-DDS hydrogels at 5%, 10%, and 15% GelMA for cefazolin doses of 3 µg, 15 µg, 30 µg, and 90 µg. (A) Equilibrium swelling ratio after 7 days of swelling in phosphate-saline buffer at 37 °C. (B) Mesh size in nm. The experiment was performed once with $n = 5-7$. **** $p < 0.0001$.

Similarly, the theoretical hydrogel mesh size decreased with increasing GelMA concentration from 5% to 15% (Figure 4B). The mesh sizes observed ranged from around 10 nm to 31 nm, which is in good agreement with other studies [26]. The dose of drug loading also significantly affected the mesh size in all GelMA concentrations. Most noticeably, the loading of 90 µg cefazolin significantly increased the mesh size of 10% GelMA. Overall, the swelling ratio and calculated mesh size indicate a potential impact of the higher doses of on the physicochemical properties of the GelMA-DDS.

Release profiles are commonly controlled by hydrogel crosslinking density and resulting mesh size [15,50,61]. Here, results showed similar release profiles and burst release for all tested GelMA concentrations, suggesting that mesh sizes, which ranged from 10 nm to 31 nm, did not influence the retention of cefazolin, which has an approximate size of 1.74 nm [45]. Therefore, even at high GelMA concentrations, the smallest mesh size was too large to retain the cefazolin drug loaded in our GelMA-DDS for prolonged periods.

Based on the results of our drug release studies, we concluded that GelMA concentration did not significantly impact the release kinetics, while the cefazolin dose did. The drug was released in a burst release within the first few hours, and the mesh sizes were too large compared to cefazolin to achieve sustained release. However, the objective is to deliver antibiotics locally and the preferred release kinetics is a burst release above the MIC of the bacteria [62]. Indeed, cefazolin release profiles from hydrogel-DDS were reported

by others and ranged from a few hours (4–5) to a few days [41,63,64] and are typically characterized by a burst release within the first few hours (1–4) [65,66], followed by an exponential decay [65]. Furthermore, approved DDS for antibiotic release use the dose factor to tailor the release profile, which denotes the primary importance of the dose factor that needs to be above the MIC of the bacteria [67,68]. Additionally, the half-life of cefazolin in the blood compartment is only 1.8–2 h [69,70]. Consequently, our GelMA-DDS provides additional protection and local availability of cefazolin.

3.2. Mechanical and Physical Properties of the Drug Delivery System

3.2.1. Mechanical Testing

When designing an implantable hydrogel-DDS, the mechanical properties of the hydrogel-DDS play a critical role in the system stability and degradability [71]. Therefore, hydrogel mechanical properties should be adaptable to tune degradation and release profiles [71]. We therefore evaluated the tuneability and impact of cefazolin loading on the mechanical properties of GelMA hydrogels. Since the GelMA concentration did not affect the release kinetics of cefazolin, we continued all further experiments with 10% GelMA and cefazolin doses between 3 and 90 μg .

Figure 5 shows the mechanical compression testing results for 10% GelMA with and without cefazolin. In the absence of cefazolin, the compressive modulus was ~ 47 kPa, as expected [72] (Figure 5A). Statistical analysis demonstrated a significant effect of the cefazolin dose on the compressive moduli of the GelMA-DDS ($p < 0.0001$). Indeed, Figure 5A shows that loading of 90 μg cefazolin in 10% GelMA hydrogel discs resulted in a significantly lower compressive modulus than the control group (~ 19 kPa) which was more similar to the typical modulus of 5% GelMA hydrogels [50,72]. The hydrogel toughness and failure stress averaged from ~ 48 to ~ 55 kJ/m^3 (Figure 5B) and ~ 462 to ~ 696 kPa (Figure 5C), respectively, which were unaffected by the cefazolin dose and comparable to previously published data [50,72]. The failure strain was not significantly different between 10% GelMA with and without cefazolin doses ranging from 3 to 30 μg . However, failure strain for the highest cefazolin dose (90 μg) was significantly higher, indicating a lower degree of crosslinking [50,72] (Figure 5D). Effective swelling, a measure of water uptake following incubation in a buffer, ranged from ~ -1 to $\sim 10\%$ but was significantly higher at the 90 μg cefazolin dose ($\sim 13\%$), further corroborating lower crosslinking densities in gels containing high doses of cefazolin [50,72] (Figure 5E).

Overall, the expected range of mechanical properties for 10% GelMA observed in our experiment was in accordance with other studies [50,72]. However, encapsulation of the highest doses of cefazolin (90 μg) decreased the compressive moduli, as well as increased the effective swelling and failure strain of GelMA-DDS. The mechanical testing results have thus confirmed and explained the observations that at a fixed GelMA concentration of 10%, higher doses of cefazolin impacted degradation time and mesh size of the final DDS (Figures 3 and 4). Because the mechanical properties of GelMA at a given concentration are dependent on the degree of crosslinking [22], we hypothesized that high concentrations of cefazolin may interfere with the crosslinking reaction. This interference could be related to cefazolin's molecular structure, which may scavenge free radicals and delay or impair the crosslinking reaction. Evidence of the free-radical scavenging potential of beta-lactam antibiotics, namely ampicillin, penicillin, oxacillin, and dicloxacillin, all belonging to the same antibiotic class as cefazolin, was reported by Berczyński et al. [73].

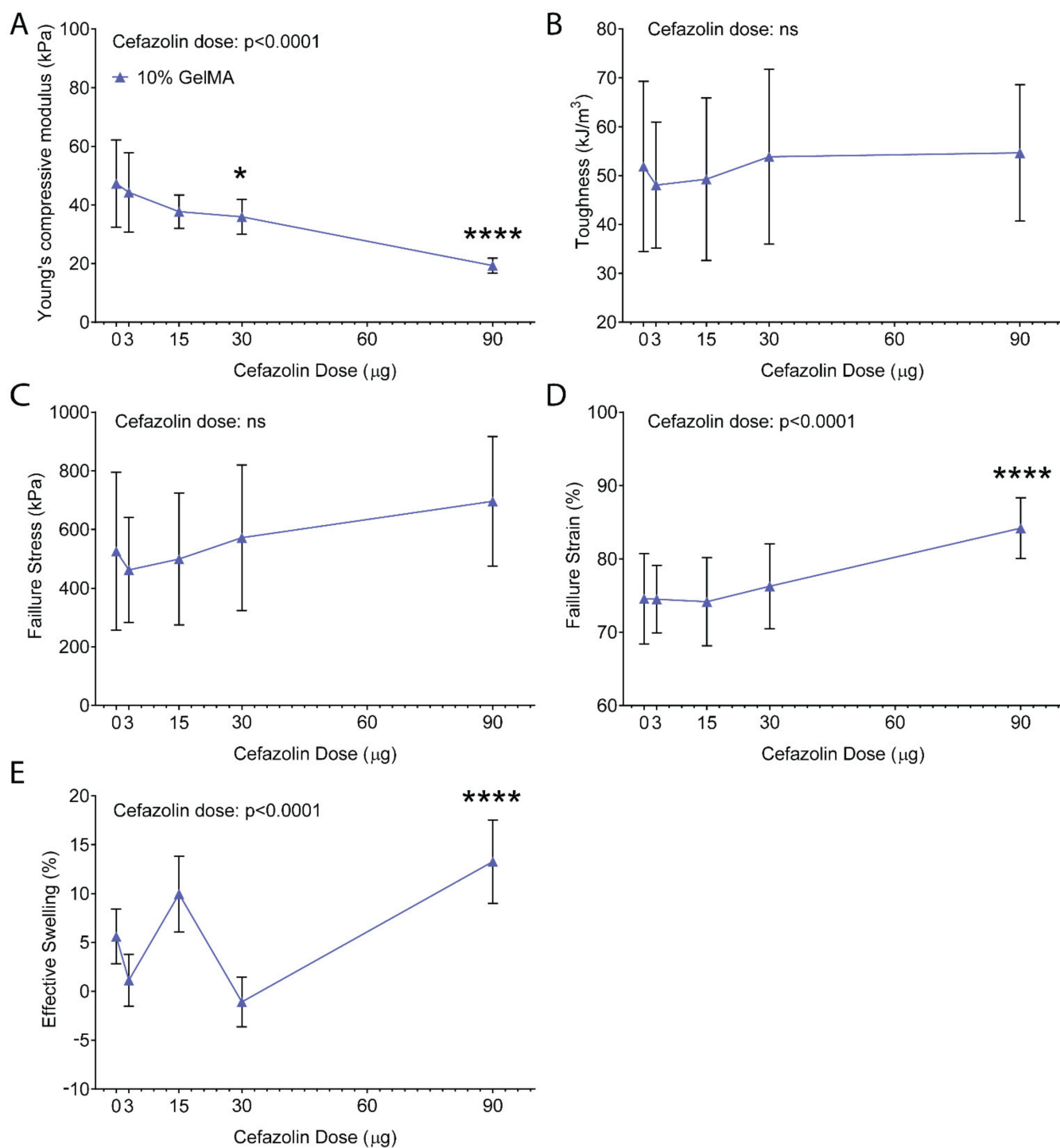


Figure 5. Compressive properties of GelMA-DDS hydrogels at 10% GelMA for cefazolin doses of 0 μg, 3 μg, 15 μg, 30 μg, and 90 μg. (A) Compressive modulus. (B) Toughness. (C) Failure stress. (D) Failure strain. (E) Effective swelling. Data are shown as mean ± standard deviation, n = 8. * p < 0.05; **** p < 0.0001. All statistical significances are with reference to the control group (10% GelMA).

3.2.2. Photorheology

Our finding that a dose of 90 μg cefazolin decreased the compressive moduli of 10% GelMA-DDS prompted us to investigate the impact of drug loading on the crosslinking reaction. We hypothesized that cefazolin may act as a radical scavenger, and GelMA crosslinking inhibition would increase in a dose-dependent manner. Photocrosslinking of GelMA-DDS was performed via free-radical polymerization using Irgacure 2959, a common photoinitiator for hydrogel systems [74]. Irgacure 2959 is a type I photoinitiator that cleaves into free radical species upon absorption of UV photons [75]. The two free radical species created are a ketyl radicals, which are short-lived, and a benzoyl radicals, which initiate a polymerization chain reaction [75,76]. While the free radical generation is dependent on the light intensity, the crosslinking reaction rate and storage modulus of the hydrogels depends on the concentration of those generated free radicals that initiate the photopolymerization reaction [77].

The photocrosslinking reaction was empirically studied in real-time by monitoring the storage modulus (G') as a function of UV exposure time (Figure 6A) for 3 to 90 μg cefazolin in 10% GelMA. We observed a delay (onset time) after the UV light was turned on before an increase in G' was detected. This onset time (~ 150 s) is attributed to the presence of oxygen in the hydrogel precursor solution, which scavenges the photoinitiator radicals [77]. This dissolved oxygen must be depleted before the crosslinking reaction is underway. The storage moduli (Figure 6A) and photocrosslinking reaction rates (Figure 6B) were inversely correlated with the encapsulated cefazolin dose. The maximum crosslinking rates, shown in Figure 6C, confirmed the dose-dependent effect of cefazolin on the crosslinking reaction rate, which decreased as a function of the increasing cefazolin dose. Collectively, this data demonstrates that the presence of high doses/concentrations of cefazolin impacted the polymerization of the GelMA-DDS.

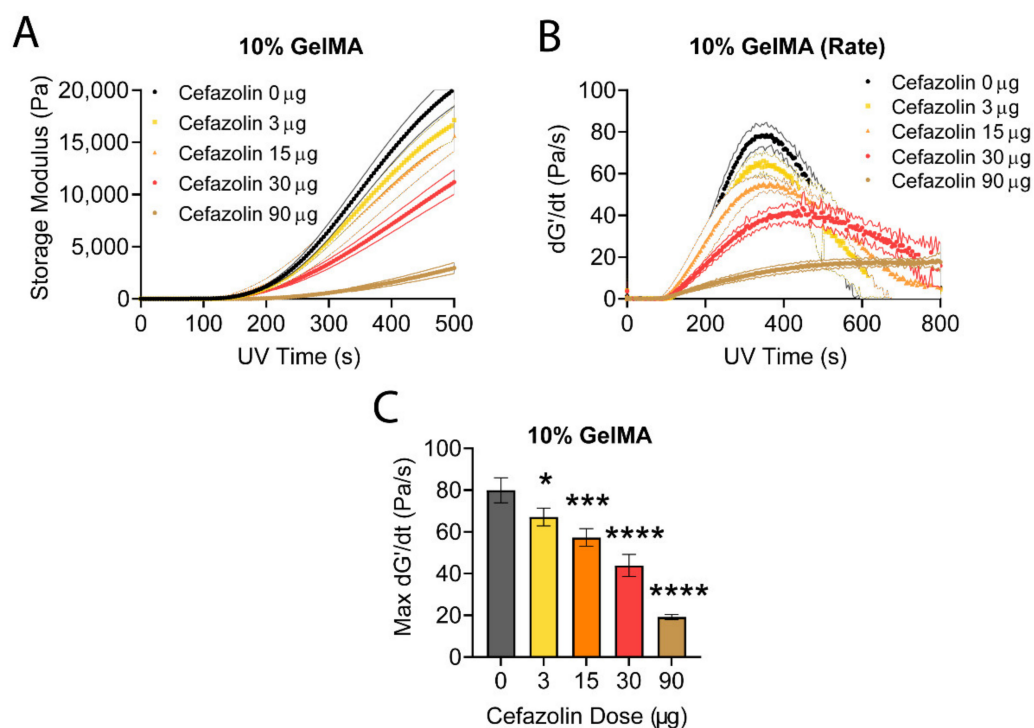


Figure 6. In situ photorheology of 10% GelMA-DDS hydrogels for the first 500 s of the crosslinking reaction. (A) Storage modulus. (B) Crosslinking reaction rate. (C) Maximum crosslinking reaction rates. Photocrosslinking with 0.5 mg/mL Irgacure 2959 at 365 nm. $n = 5$ samples for all groups. Error bands indicated the standard deviation for A and B. For C, symbols indicate statistical differences compared to the control group without cefazolin (* $p < 0.05$, *** $p < 0.001$, **** $p < 0.0001$).

There may be different explanations for this observation. In free-radical polymerizations, the rate of propagation (R_p) is proportional to the square root of the rate of initiation (R_i) [78], according to:

$$R_p = k_p[M] \left(\frac{R_i}{2k_t} \right)^{\frac{1}{2}} \quad (7)$$

Here $[M]$ is the concentration of monomer, k_p is the rate constant for propagation, and k_t is the rate constant for termination. The rate of initiation is given by [78]:

$$R_i = \frac{2\phi\epsilon f \lambda I c_i}{N_A h c} \quad (8)$$

where ϕ is the quantum yield of photolysis i.e., the fraction of absorbed photons that cleave a photoinitiator molecule (0.29); ϵ is the molar extinction coefficient ($2.46 \text{ M}^{-1} \text{ cm}^{-1}$ [77]); f is the photoinitiator efficiency (the ratio of initiation events to radicals generated by photolysis); λ is the wavelength of light (365 nm); I is the intensity of light (0.003 W/cm^2 [77]); c_i is the instantaneous molar concentration of photoinitiator molecules ($2.23 \times 10^{-3} \text{ M}$); N_A is Avogadro's constant ($6.022 \times 10^{23} \text{ mol}^{-1}$); h is Planck's constant ($6.63 \times 10^{-34} \text{ m}^2 \text{ kg/s}$); c is the speed of light ($299,792,458 \text{ m/s}$).

There are three factors from the two previously mentioned equations (Equations (7) and (8)) that may be affected by the loading of cefazolin in GelMA: the light intensity I , the photoinitiator efficiency f , and the rate of termination k_t . Firstly, the light intensity I ; this is unlikely to be affected by the cefazolin loading since the UV-Vis spectrum of cefazolin shows negligible absorbance at 365 nm [79]. Secondly, the photoinitiator efficiency f ; if free radicals reacted with the drug, this would reduce the proportion available to initiate crosslinking. In that case, the reaction rate should show a square root dependence on the cefazolin concentration. Thirdly, if the radicalized GelMA molecules reacted with the drug, this might increase the rate of termination k_t . This would reduce the rate of crosslinking, may also reduce the final storage modulus achieved, and would also display a crosslinking rate dependent on the square root dependence on the cefazolin concentration. Considering the relative concentrations and mobilities of each species, we suspect the photoinitiator efficiency is the parameter most likely affected by cefazolin loading.

To investigate our hypothesis, the crosslinking rates were normalized to the control group, 10% GelMA containing no cefazolin, and plotted against the square root of the cefazolin doses (Figure 7). The reaction rates show a linear dependence with the square root of the cefazolin concentration, as it would be expected if cefazolin is reacting with some of the initializing free radicals. The linear regression fit in Figure 7 confirmed the relationship with an R^2 superior to 0.99.

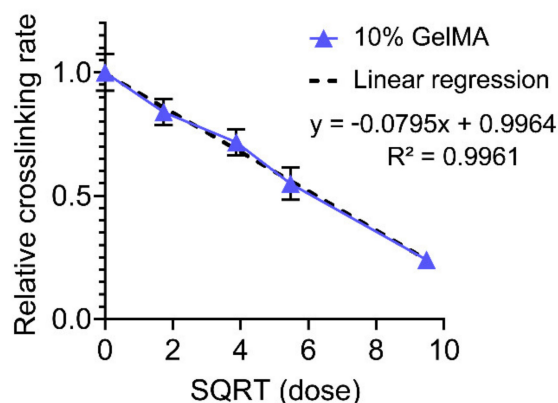


Figure 7. 10% GelMA crosslinking rate normalized to the control sample (no cefazolin) versus the square roots of cefazolin doses. Linear regression fit showing good agreement: $R^2 = 0.9961$.

Once we confirmed the impact of the cefazolin loading on the crosslinking rate and the photoinitiator efficiency f (proportional to the square root of the crosslinking rate), we then mathematically estimated the proportion of cefazolin molecules consumed by free radicals [77] (Table 2).

Table 2. Proportion of cefazolin molecules potentially consumed during crosslinking reaction.

Cefazolin Dose (μg)	Cefazolin Concentration (M)	Relative Crosslinking Rate (%)	Photoinitiator Efficiency f :	Effective Rate of Free Radical Generation (M/s)	Cumulative Consumed Radicals (M) at $t = 1800\text{s}$	Proportion of Drug Consumed	Mass of Drug Consumed (ng)
0	0	1.00	1	3.33×10^{-8}	0.0	0.00%	0
3	1.89×10^{-4}	0.81	0.9	3.00×10^{-8}	5.9×10^{-6}	3.14%	94.20
15	9.43×10^{-4}	0.69	0.8307	2.77×10^{-8}	1.0×10^{-5}	1.07%	160.50
30	1.89×10^{-3}	0.59	0.7681	2.56×10^{-8}	1.4×10^{-5}	0.72%	216.00
90	5.66×10^{-3}	0.24	0.4899	1.63×10^{-8}	3.0×10^{-5}	0.53%	477.00

The in situ photorheology characterization indicated a significant and robust relationship between cefazolin concentration and the rate of the photocrosslinking reaction. While the radicalized initiators may be reacting with cefazolin, reducing the effective concentration of initiating free radicals, the effect on the cefazolin loading was limited to a maximum of 3% of the cefazolin that would be consumed by free radicals. This result implies that a maximum of ~90 ng out of the 3 μg of cefazolin would be consumed, while ~480 ng from the 90 μg of cefazolin would be consumed.

Furthermore, while all cefazolin doses impacted the crosslinking reaction rate in a dose-dependent manner, only the highest dose of 90 μg of cefazolin significantly decreased the final physicochemical properties of the GelMA-DDS in the fully crosslinked hydrogels (Figure 5).

3.3. In Vitro Evaluation of GelMA-DDS

3.3.1. Diffusive Zone of Inhibition Assay

The efficacy of the prophylactic release of cefazolin from GelMA was first assessed against *S. aureus*, one of the main pathogens involved in the SSI incidence [3], using a zone inhibition assay (Figure 8). Representative images of the zone of inhibition for all tested groups are presented in Figure 8A,B. As expected, the zone of inhibition increased in a dose-dependent manner from 3 μg , 15 μg , 30 μg , and 90 μg released from 10% GelMA hydrogels following a logarithmic function (Figure 8C,D). A similar dose-dependency effect of cefazolin was observed when the antibiotic was released from polycaprolactone scaffolds in another study [80]. Additionally, the 30- μg cefazolin dose had a similar efficiency compared to the positive control with the same dose loaded; thus, the cefazolin bioactivity was not altered despite small amounts of cefazolin being consumed during the photocrosslinking reaction (Table 2).

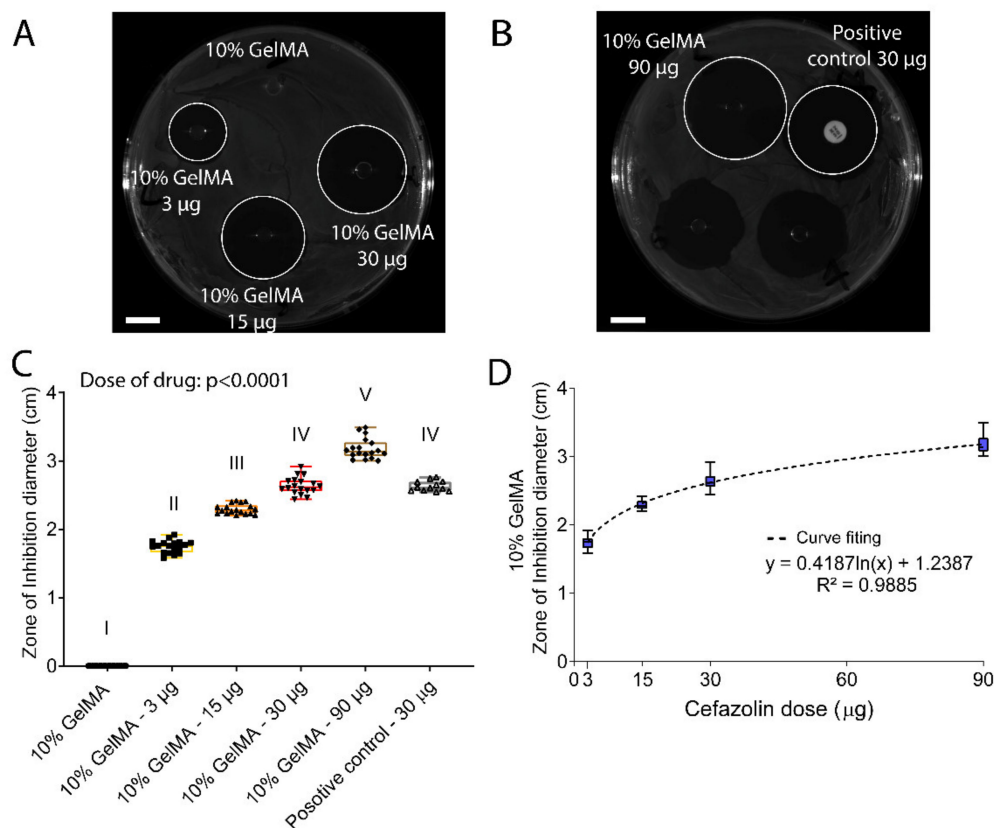


Figure 8. In vitro evaluation of 10% GelMA-DDS efficacy against *S. aureus* in a zone of inhibition assay. *S. aureus* was spread on Petri dishes containing Mueller-Hinton agar, then samples were placed on the culture plate and left incubating at 37 °C overnight. (A,B) Representative pictures of Petri dishes at the end of the assay. Scale bar = 1 cm. (C) Zone of inhibition in cm. Results are shown as box plots. Groups with no statistical difference are marked with the same roman numeral. (D) Non-linear regression for GelMA 10% versus cefazolin doses. The experiment was performed three times with $n = 6$ each time.

3.3.2. Broth Growth Inhibition Assay

The zone of inhibitions assay was complemented by a broth inhibition assay designed based on the microdilution susceptibility assay [81]. The goal was to assess the antibacterial efficacy of cefazolin loaded GelMA-DDS against *S. aureus* in suspension and over time [40,82]. Figure 9 shows that the dose was a significant factor affecting *S. aureus* growth inhibition. A cefazolin dose of 3 µg inhibited bacteria growth for 1 day only, while the doses 15 µg and 30 µg both inhibited bacteria growth for 2 days, and 90 µg of cefazolin prevented bacteria growth for 3 days. Additionally, the cefazolin dose of 30 µg showed similar antibacterial efficacy compared to the positive control of cefazolin 30 µg on day 0. In this assay, we saw a prolonged antibacterial effect of cefazolin for up to several days, while the diffusive release assay performed earlier showed that most of the drug cargo was released within hours (Figure 2). The MIC of cefazolin for *S. aureus* ATCC29213 inoculated at 5×10^6 CFU/mL is close to 1 µg/mL [37]. Assuming that the cefazolin concentration in GelMA and the media were in equilibrium, a fraction of the cefazolin dose would remain in GelMA after day 1. These fractions are equivalent to 6.3 µg, 2.1 µg, 1.05 µg, and 0.21 µg, for total drug doses of 90 µg, 30 µg, 15 µg, and 3 µg, respectively. Therefore, cefazolin amounts remaining in the hydrogel-DDS on day 2 were all above the MIC except for the lowest dose of 3 µg cefazolin, resulting in the observed antibacterial effects. Additionally, contrary to the diffusive release in PBS (Figure 2), where the release media was refreshed four times during the first 24 h which would induce an overall higher osmotic pressure

Phosphate-buffered saline (PBS) solution and in a collagenase II and Hank's Balanced Salt Solution (HBSS). The standard curves covered the range of 1.95 ppb = ng/mL to 1000 ppb = 1000 ng/mL. (A) Standard curve. (B) Column comparison.; Figure S2. Cefazolin diffusive in vitro release in phosphate-buffered saline at pH 7.4, under 75 rpm agitation at 37 °C. 3 µg, 15 µg, 30 µg, and 90 µg cefazolin were released from 5%, 10%, and 15% GelMA. (A) Cefazolin total release in µg. (B) Fraction of cefazolin released per timepoint expressed in µg.; Figure S3. Gelatin methacryloyl hydrogel at 5%, 10%, and 15% concentration loaded with cefazolin 3 µg, 15 µg, 30 µg, and 90 µg were swelled in phosphate-buffered saline at pH 7.4 for 7 days to ensure reaching the equilibrium swelling. (A) Weight of the hydrogels at equilibrium swelling. (B) Weight of the hydrogels after lyophilization. N = 5–7.; Figure S4. Compressive properties of GelMA-DDS hydrogels at 5%, 10%, and 15% GelMA for cefazolin doses of 0 µg, 3 µg, 15 µg, 30 µg, and 90 µg. (A) Compressive modulus. (B) Toughness. (C) Failure stress. (D) Failure strain. (E) Effective swelling. Data are shown as mean ± standard deviation, n = 8. The mention 'GelMA concentration X Cefazolin dose' signifies that the interaction of both parameters is significant. * $p < 0.05$; *** $p < 0.001$, **** $p < 0.0001$. All statistical significances are with reference to the respective control groups: 5% GelMA, 10% GelMA, 15% GelMA. # indicates a significant difference between 5% GelMA + Cefazolin 30 µg and 5% GelMA.; Figure S5. In situ photorheology for 5%, 10%, and 15% GelMA containing cefazolin with 0.5% Irgacure2959 photoinitiator. (A) Raw data for 5% GelMA, 5% GelMA + 30 µg of cefazolin, and 5% GelMA + 90 µg of cefazolin. (B) Raw data for 10% GelMA, 10% GelMA + 3 of µg cefazolin, 10% GelMA + 15 of µg cefazolin, 10% GelMA + 30 of µg cefazolin, and 10% GelMA + 90 of µg cefazolin. (C) Raw data for 15% GelMA, 15% GelMA + 30 µg of cefazolin, and 15% GelMA + 90 µg of cefazolin.; Figure S6. In situ photorheology of GelMA-DDS hydrogels for the first 500 s of the crosslinking reaction. (A) 5% GelMA storage modulus. (B) 5% GelMA crosslinking reaction rate. (C) 15% GelMA storage modulus. (D) 15% GelMA crosslinking reaction rate. (E) 5% GelMA maximum crosslinking reaction rates. (F) 15% GelMA maximum crosslinking reaction rates. Photocrosslinking with 0.5 mg/mL Irgacure 2959 at 365 nm. n = 5 for all 5% GelMA and n = 2 for all 15% GelMA samples. Error bands indicated the standard deviation for A to D. For E, symbols indicate statistical differences compared to control groups without cefazolin (* $p < 0.05$; ** $p < 0.01$, *** $p < 0.001$, **** $p < 0.0001$); Figure S7. Normalized crosslinking rates against the control sample (no cefazolin) at 5% and 15% GelMA. (A) Relative crosslinking rate versus the square roots of cefazolin doses. (B) Linear regression fit showing good agreement: $R^2 = 0.995$.; Figure S8. Free radicals used for the crosslinking reaction. (A) Photoinitiator degradation model in a 1 cm cube. Incident light intensity (in einsteins $s^{-1} cm^{-2}$) × fraction of light absorbed × quantum yield = degradation rate of photo-initiator (in moles s^{-1}). Modified from [1]. (B) Estimate of I2959 radicals generated as a function of time for in absence of cefazolin 0 µg and for the different cefazolin doses, 3 µg, 15 µg, 30 µg, and 90 µg, using the respective photoinitiator efficiencies.; Figure S9. In vitro evaluation of 5% and 15% GelMA-DDS efficacy against *S. aureus* in a zone of inhibition assay. *S. aureus* was spread on Petri dishes containing Mueller-Hinton agar, then samples were placed on the culture plate and left incubating at 37 °C overnight. (A) and (B) Representative pictures of Petrie dishes at the end of the assay. Scale bar = 1 cm. (C) Zone of inhibition in cm. Results are shown as box plots. Groups with no statistical difference are marked with the same roman numeral. The experiment was performed three times with n = 6 each time.; Figure S10. In vitro evaluation of 10% GelMA-DDS efficacy against broth culture of *S. aureus*. A 0.5 McFarland of *S. aureus* suspension in MH broth was prepared and diluted 100 times to reach 5×10^6 CFU/mL. The broth suspension was added to each well to start the assay (0.5 mL per well), and a new broth solution was prepared every day, at every timepoint except for the last one, to refresh the bacteria solution. Optical density was measured at 600 nm each day for all groups: 30 µg cefazolin in 5%, 10%, and 15% GelMA. Control groups were added: 10% GelMA = negative control; *S. aureus* = negative control; positive control disc containing cefazolin 30 µg. Data are shown as mean ± SD. The experiment was performed three times with n = 6.

Author Contributions: M.V., C.M., N.B. and D.W.H. conceived and designed the experiments. M.V., C.D.O. and S.C. conducted the experiments. M.V., D.W.H., C.M. and N.B. wrote the paper. All authors have read and agreed to the published version of the manuscript.

Funding: D.W.H. is thankful for the financial support provided by the Australian Research Council (ARC) Training Centre for Cell and Tissue Engineering Technologies (IC190100026), the ARC Training Centre in Additive Biomanufacturing (IC160100026), and the ARC Training Centre for Multiscale 3D Imaging, Modelling and Manufacturing (IC180100008). N.B is thankful for support from JJ Richards

& Sons via an In Vitro Excellence Research grant, Advance Queensland via an Advance Queensland Industry Research Fellowship (AQIRF066-2019RD2), and the ARC Training Centre for Multiscale 3D Imaging, Modelling and Manufacturing (IC180100008).

Data Availability Statement: The data presented in this study are available on request from the corresponding authors.

Conflicts of Interest: C.M. and D.W.H. are Co-Founders of Gelomics Pty Ltd., a Brisbane-based biotechnology company distributing hydrogel kits for 3D cell culture applications. C.M. is also Managing Director of Gelomics Pty Ltd.

References

1. Lamagni, T. Epidemiology and burden of prosthetic joint infections. *J. Antimicrob. Chemother.* **2014**, *69*, i5–i10. [[CrossRef](#)] [[PubMed](#)]
2. Reichman, D.E.; A Greenberg, J. Reducing Surgical Site Infections: A Review. *Rev. Obstet. Gynecol.* **2009**, *2*, 212–221. [[PubMed](#)]
3. Owens, C.; Stoessel, K. Surgical site infections: Epidemiology, microbiology and prevention. *J. Hosp. Infect.* **2008**, *70*, 3–10. [[CrossRef](#)]
4. Weichman, K.E.; Levine, S.M.; Wilson, S.C.; Choi, M.; Karp, N. Antibiotic Selection for the Treatment of Infectious Complications of Implant-Based Breast Reconstruction. *Ann. Plast. Surg.* **2013**, *71*, 140–143. [[CrossRef](#)]
5. Kusaba, T. Safety and Efficacy of Cefazolin Sodium in the Management of Bacterial Infection and in Surgical Prophylaxis. *Clin. Med. Ther.* **2009**, *1*, CMT.S2096. [[CrossRef](#)]
6. Bratzler, D.W.; Houck, P.M. Antimicrobial prophylaxis for surgery: An advisory statement from the National Surgical Infection Prevention Project. *Am. J. Surg.* **2005**, *189*, 395–404. [[CrossRef](#)]
7. Macdonald, D.J.; Gray, A.J.R. Methicillin-resistant Staphylococcus aureus in trauma and orthopaedic practice. *J. Bone Jt. Surg. Br. Vol.* **2006**, *88*, 137–138. [[CrossRef](#)]
8. Yotsuji, A.; Mitsuyama, J.; Hori, R.; Yasuda, T.; Saikawa, I. Mechanism of Action of Cephalosporins and Resistance Caused by Decreased Affinity for Penicillin-Binding Proteins in Bacteroides fragilis. *Antimicrob. Agents Chemother.* **1988**, *32*, 1848–1853. [[CrossRef](#)]
9. Oates, J.A.; Wood, A.J.; Donowitz, G.R.; Mandell, G.L. Beta-Lactam Antibiotics. *N. Engl. J. Med.* **1988**, *318*, 490–500. [[CrossRef](#)]
10. Singh, R.; Sripada, L.; Singh, R. Side effects of antibiotics during bacterial infection: Mitochondria, the main target in host cell. *Mitochondrion* **2014**, *16*, 50–54. [[CrossRef](#)]
11. Cunha, B.A. Antibiotic Side Effects. *Med. Clin. N. Am.* **2001**, *85*, 149–185. [[CrossRef](#)]
12. Fair, R.J.; Tor, Y. Antibiotics and Bacterial Resistance in the 21st Century. *Perspect. Med. Chem.* **2014**, *6*, PMC–S14459. [[CrossRef](#)]
13. Brooks, B.D.; Brooks, A.E. Therapeutic strategies to combat antibiotic resistance. *Adv. Drug Deliv. Rev.* **2014**, *78*, 14–27. [[CrossRef](#)]
14. Kohrs, N.J.; Liyanage, T.; Venkatesan, N.; Najarzadeh, A.; Puleo, D.A. Drug Delivery Systems and Controlled Release. *Biomed. Sci.* **2019**, *2*, 316–329.
15. Li, J.; Mooney, D.J. Designing hydrogels for controlled drug delivery. *Nat. Rev. Mater.* **2016**, *1*, 1–17. [[CrossRef](#)]
16. Mazzeo, L.; Bianchi, M.; Cocchi, M.; Piemonte, V. Drug Delivery with Membranes Systems. In *Current Trends and Future Developments on (Bio-) Membranes*; Elsevier: Amsterdam, The Netherlands, 2019; pp. 291–309. [[CrossRef](#)]
17. Abedini, F.; Ebrahimi, M.; Roozbehani, A.H.; Domb, A.J.; Hosseinkhani, H. Overview on natural hydrophilic polysaccharide polymers in drug delivery. *Polym. Adv. Technol.* **2018**, *29*, 2564–2573. [[CrossRef](#)]
18. Sercombe, L.; Veerati, T.; Moheimani, F.; Wu, S.; Sood, A.K.; Hua, S. Advances and Challenges of Liposome Assisted Drug Delivery. *Front. Pharmacol.* **2015**, *6*, 286. [[CrossRef](#)]
19. Zhang, Y.S.; Khademhosseini, A. Advances in engineering hydrogels. *Science* **2017**, *356*. [[CrossRef](#)]
20. Loessner, D.; Meinert, C.; Kaemmerer, E.; Martine, L.; Yue, K.; Levett, P.A.; Klein, T.; Melchels, F.P.W.; Khademhosseini, A.; Hutmacher, D.W. Functionalization, preparation and use of cell-laden gelatin methacryloyl-based hydrogels as modular tissue culture platforms. *Nat. Protoc.* **2016**, *11*, 727–746. [[CrossRef](#)]
21. Zhu, M.; Wang, Y.; Ferracci, G.; Zheng, J.; Cho, N.-J.; Lee, B.H. Gelatin methacryloyl and its hydrogels with an exceptional degree of controllability and batch-to-batch consistency. *Sci. Rep.* **2019**, *9*, 1–13. [[CrossRef](#)]
22. Miri, A.K.; Hosseinabadi, H.G.; Cecen, B.; Hassan, S.; Zhang, Y.S. Permeability mapping of gelatin methacryloyl hydrogels. *Acta Biomater.* **2018**, *77*, 38–47. [[CrossRef](#)] [[PubMed](#)]
23. Luo, Z.; Sun, W.; Fang, J.; Lee, K.; Li, S.; Gu, Z.; Dokmeci, M.R.; Khademhosseini, A. Biodegradable Gelatin Methacryloyl Microneedles for Transdermal Drug Delivery. *Adv. Health Mater.* **2018**, *8*, e1801054. [[CrossRef](#)] [[PubMed](#)]
24. Peppas, N.A.; Merrill, E.W. Crosslinked poly(vinyl alcohol) hydrogels as swollen elastic networks. *J. Appl. Polym. Sci.* **1977**, *21*, 1763–1770. [[CrossRef](#)]
25. Canal, T.; Peppas, N.A. Correlation between mesh size and equilibrium degree of swelling of polymeric networks. *J. Biomed. Mater. Res.* **1989**, *23*, 1183–1193. [[CrossRef](#)]
26. Gilchrist, A.E.; Lee, S.; Hu, Y.; Harley, B.A.C. Mesenchymal stromal cell remodeling of a gelatin hydrogel microenvironment defines an artificial hematopoietic stem cell niche. *BioRxiv* **2018**, 289553. [[CrossRef](#)]

27. Berg, J.M.; Tymoczko, J.L.; Stryer, L. Primary Structure: Amino Acids Are Linked by Peptide Bonds to Form Polypeptide Chains. In *Biochemistry*, 5th ed.; W. H. Freeman: New York, NY, USA, 2002; p. 1100.
28. Fels, I.G. Hydration and density of collagen and gelatin. *J. Appl. Polym. Sci.* **1964**, *8*, 1813–1824. [[CrossRef](#)]
29. Fessler, J.; Hodge, A. Ultracentrifugal observation of phase transitions in density gradients: I. The collagen system. *J. Mol. Biol.* **1962**, *5*, 446–449. [[CrossRef](#)]
30. Anjum, F.; Lienemann, P.S.; Metzger, S.; Biernaskie, J.; Kallos, M.S.; Ehrbar, M. Enzyme responsive GAG-based natural-synthetic hybrid hydrogel for tunable growth factor delivery and stem cell differentiation. *Biomaterials* **2016**, *87*, 104–117. [[CrossRef](#)]
31. Schiel, J.E.; Hage, D.S. Density measurements of potassium phosphate buffer from 4 to 45 °C. *Talanta* **2005**, *65*, 495–500. [[CrossRef](#)]
32. Flory, P.J.; Rehner, J. Statistical Mechanics of Cross-Linked Polymer Networks I. Rubberlike Elasticity. *J. Chem. Phys.* **1943**, *11*, 512–520. [[CrossRef](#)]
33. Bray, J.C.; Merrill, E.W. Poly(vinyl alcohol) hydrogels. Formation by electron beam irradiation of aqueous solutions and subsequent crystallization. *J. Appl. Polym. Sci.* **1973**, *17*, 3779–3794. [[CrossRef](#)]
34. Ofner, I.C.M.; Bubnis, W.A. Chemical and Swelling Evaluations of Amino Group Crosslinking in Gelatin and Modified Gelatin Matrices. *Pharm. Res.* **1996**, *13*, 1821–1827. [[CrossRef](#)]
35. Kasapis, S.; Al-Marhoobi, I.M.; Mitchell, J.R. Molecular weight effects on the glass transition of gelatin/cosolute mixtures. *Biopolymers* **2003**, *70*, 169–185. [[CrossRef](#)]
36. Kahl, M.; Schneidereit, D.; Bock, N.; Friedrich, O.; Hutmacher, D.W.; Meinert, C. MechAnalyze—An algorithm for standardization and automation of compression test analysis. *Tissue Eng. Part C Methods* **2021**, *27*, 529–542. [[CrossRef](#)]
37. Hudzicki, J. Kirby-Bauer Disk Diffusion Susceptibility Test Protocol. *Am. Soc. Microbiol.* **2009**, *66*, 208.
38. Nannini, E.; Stryjewski, M.; Singh, K.V.; Bourgogne, A.; Rude, T.H.; Corey, G.R.; Fowler, V.G.; Murray, B.E. Inoculum Effect with Cefazolin among Clinical Isolates of Methicillin-Susceptible *Staphylococcus aureus*: Frequency and Possible Cause of Cefazolin Treatment Failure. *Antimicrob. Agents Chemother.* **2009**, *53*, 3437–3441. [[CrossRef](#)]
39. Chen, Y.-C.; Lin, R.-Z.; Qi, H.; Yang, Y.; Bae, H.; Melero-Martin, J.M.; Khademhosseini, A. Functional Human Vascular Network Generated in Photocrosslinkable Gelatin Methacrylate Hydrogels. *Adv. Funct. Mater.* **2012**, *22*, 2027–2039. [[CrossRef](#)]
40. Shah, S.R.; Henslee, A.M.; Spicer, P.P.; Yokota, S.; Petrichenko, S.; Allahabadi, S.; Bennett, G.N.; Wong, M.E.; Kasper, F.; Mikos, A.G. Effects of Antibiotic Physicochemical Properties on Their Release Kinetics from Biodegradable Polymer Microparticles. *Pharm. Res.* **2014**, *31*, 3379–3389. [[CrossRef](#)]
41. Shahzad, A.; Khan, A.; Afzal, Z.; Umer, M.F.; Khan, J.; Khan, G.M. Formulation development and characterization of cefazolin nanoparticles-loaded cross-linked films of sodium alginate and pectin as wound dressings. *Int. J. Biol. Macromol.* **2019**, *124*, 255–269. [[CrossRef](#)]
42. Lai, P.-L.; Hong, D.-W.; Ku, K.-L.; Lai, Z.-T.; Chu, I.-M. Novel thermosensitive hydrogels based on methoxy polyethylene glycol-co-poly(lactic acid-co-aromatic anhydride) for cefazolin delivery. *Nanomed. Nanotechnol. Biol. Med.* **2014**, *10*, 553–560. [[CrossRef](#)]
43. Mantripragada, V.P.; Jayasuriya, A.C. Effect of dual delivery of antibiotics (vancomycin and cefazolin) and BMP-7 from chitosan microparticles on *Staphylococcus epidermidis* and pre-osteoblasts in vitro. *Mater. Sci. Eng. C* **2016**, *67*, 409–417. [[CrossRef](#)]
44. Arya, A.D.; Hallur, P.M.; Karkisaval, A.G.; Gudipati, A.; Rajendiran, S.; Dhavale, V.; Ramachandran, B.; Jayaprakash, A.; Gundiah, N.; Chaubey, A. Gelatin Methacrylate Hydrogels as Biomimetic Three-Dimensional Matrixes for Modeling Breast Cancer Invasion and Chemoresponse in Vitro. *ACS Appl. Mater. Interfaces* **2016**, *8*, 22005–22017. [[CrossRef](#)]
45. National Center for Biotechnology Information. PubChem Compound Summary for CID 23675322, Cefazolin sodium. Retrieved 15 November 2021. 2021. Available online: <https://pubchem.ncbi.nlm.nih.gov/compound/Cefazolin-sodium> (accessed on 27 October 2021).
46. National Center for Biotechnology Information. PubChem Compound Summary for CID 31703, Doxorubicin. Retrieved 15 November 2021. 2021. Available online: <https://pubchem.ncbi.nlm.nih.gov/compound/Doxorubicin> (accessed on 27 October 2021).
47. Park, J.H.; Kwon, S.; Lee, M.; Chung, H.; Kim, J.-H.; Kim, Y.-S.; Park, R.-W.; Kim, I.-S.; Seo, S.B.; Kwon, I.C.; et al. Self-assembled nanoparticles based on glycol chitosan bearing hydrophobic moieties as carriers for doxorubicin: In vivo biodistribution and anti-tumor activity. *Biomaterials* **2006**, *27*, 119–126. [[CrossRef](#)]
48. Calori, I.R.; Braga, G.; Jesus, P.D.C.C.D.; Bi, H.; Tedesco, A.C. Polymer scaffolds as drug delivery systems. *Eur. Polym. J.* **2020**, *129*, 109621. [[CrossRef](#)]
49. Nichol, J.W.; Koshy, S.; Bae, H.; Hwang, C.M.; Yamanlar, S.; Khademhosseini, A. Cell-laden microengineered gelatin methacrylate hydrogels. *Biomaterials* **2010**, *31*, 5536–5544. [[CrossRef](#)]
50. Vigata, M.; Meinert, C.; Pahoff, S.; Bock, N.; Hutmacher, D.W. Gelatin Methacryloyl Hydrogels Control the Localized Delivery of Albumin-Bound Paclitaxel. *Polymers* **2020**, *12*, 501. [[CrossRef](#)]
51. Pepelanova, I.; Kruppa, K.; Scheper, T.; Lavrentieva, A. Gelatin-Methacryloyl (GelMA) Hydrogels with Defined Degree of Functionalization as a Versatile Toolkit for 3D Cell Culture and Extrusion Bioprinting. *Bioengineering* **2018**, *5*, 55. [[CrossRef](#)]
52. Lee, B.H.; Shirahama, H.; Kim, M.H.; Lee, J.H.; Cho, N.-J.; Tan, L.P. Colloidal templating of highly ordered gelatin methacryloyl-based hydrogel platforms for three-dimensional tissue analogues. *NPG Asia Mater.* **2017**, *9*, e412. [[CrossRef](#)]
53. Yoon, H.J.; Shin, S.R.; Cha, J.M.; Lee, S.-H.; Kim, J.-H.; Do, J.T.; Song, H.; Bae, H. Cold Water Fish Gelatin Methacryloyl Hydrogel for Tissue Engineering Application. *PLoS ONE* **2016**, *11*, e0163902. [[CrossRef](#)]

54. Chiarappa, G.; Abrami, M.; Farra, R.; Dapas, B.; Grassi, G.; Grassi, M. Drug delivery from polymeric matrices. *Comput. Aided Chem. Eng.* **2018**, *42*, 325–356. [CrossRef]
55. Lin, C.C.; Metters, A.T. Hydrogels in controlled release formulations: Network design and mathematical modeling. *Adv Drug Deliv Rev.* **2006**, *58*, 1379–1408. [CrossRef] [PubMed]
56. Mäder, K.; Lehner, E.; Liebau, A.; Plontke, S.K. Controlled drug release to the inner ear: Concepts, materials, mechanisms, and performance. *Hear. Res.* **2018**, *368*, 49–66. [CrossRef]
57. Van de Manacker, F.; Braeckmans, K.; el Morabit, N.; De Smedt, S.C.; van Nostrum, C.F.; Hennink, W.E. Protein-Release Behavior of Self-Assembled PEG- β -Cyclodextrin/PEG-Cholesterol Hydrogels. *Adv. Funct. Mater.* **2009**, *19*, 2992–3001. [CrossRef]
58. Rehmann, M.S.; Skeens, K.M.; Kharkar, P.; Ford, E.M.; Maverakis, E.; Lee, K.H.; Kloxin, A.M. Tuning and Predicting Mesh Size and Protein Release from Step Growth Hydrogels. *Biomacromolecules* **2017**, *18*, 3131–3142. [CrossRef] [PubMed]
59. Wisniewska, M.A.; Seland, J.G.; Wang, W. Determining the scaling of gel mesh size with changing crosslinker concentration using dynamic swelling, rheometry, and PGSE NMR spectroscopy. *J. Appl. Polym. Sci.* **2018**, *135*, 46695. [CrossRef]
60. Aston, R.; Sewell, K.; Klein, T.; Lawrie, G.; Grøndahl, L. Evaluation of the impact of freezing preparation techniques on the characterisation of alginate hydrogels by cryo-SEM. *Eur. Polym. J.* **2016**, *82*, 1–15. [CrossRef]
61. Ma, X.; Xu, T.; Chen, W.; Qin, H.; Chi, B.; Ye, Z. Injectable hydrogels based on the hyaluronic acid and poly (γ -glutamic acid) for controlled protein delivery. *Carbohydr. Polym.* **2018**, *179*, 100–109. [CrossRef] [PubMed]
62. Wu, P.; Grainger, D.W. Drug/device combinations for local drug therapies and infection prophylaxis. *Biomaterials* **2006**, *27*, 2450–2467. [CrossRef]
63. Mahdavinia, G.R.; Hosseini, R.; Darvishi, F.; Sabzi, M. The release of cefazolin from chitosan/polyvinyl alcohol/sepiolite nanocomposite hydrogel films. *Iran. Polym. J.* **2016**, *25*, 933–943. [CrossRef]
64. Overstreet, D.J.; Huynh, R.; Jarbo, K.; McLemore, R.Y.; Vernon, B.L. In situ forming, resorbable graft copolymer hydrogels providing controlled drug release. *J. Biomed. Mater. Res. Part A* **2013**, *101A*, 1437–1446. [CrossRef]
65. Aiken, S.S.; Cooper, J.J.; Florance, H.; Robinson, M.; Michell, S. Local Release of Antibiotics for Surgical Site Infection Management Using High-Purity Calcium Sulfate: An In Vitro Elution Study. *Surg. Infect.* **2015**, *16*, 54–61. [CrossRef]
66. Cooper, J.J.; Florance, H.; McKinnon, J.L.; Laycock, P.A.; Aiken, S.S. Elution profiles of tobramycin and vancomycin from high-purity calcium sulphate beads incubated in a range of simulated body fluids. *J. Biomater. Appl.* **2016**, *31*, 357–365. [CrossRef]
67. Howlin, R.P.; Brayford, M.J.; Webb, J.; Cooper, J.J.; Aiken, S.S.; Stoodley, P. Antibiotic-Loaded Synthetic Calcium Sulfate Beads for Prevention of Bacterial Colonization and Biofilm Formation in Periprosthetic Infections. *Antimicrob. Agents Chemother.* **2014**, *59*, 111–120. [CrossRef]
68. Sean Aiken. Assessing the Influence of Third Body Damage to Articulating Surfaces with Bone Void Fillers [Internet]. 2019 [cited 2021 Nov 16]. Available online: <https://www.biocomposites.com/wp-content/uploads/2019/08/International-Assessing-the-influence-of-third-body-damage-to-articulating-surfaces-with-bone-void-fillers-paper-MA0175R2.pdf> (accessed on 27 October 2021).
69. Bergeron, M.G.; Bruschi, J.L.; Barza, M.; Weinstein, L. Bactericidal Activity and Pharmacology of Cefazolin. *Antimicrob. Agents Chemother.* **1973**, *4*, 396–401. [CrossRef]
70. Ficker, L.; Meredith, T.A.; Gardner, S.; Wilson, L.A. Cefazolin levels after intravitreal injection. Effects of inflammation and surgery. *Investig. Ophthalmol. Vis. Sci.* **1990**, *31*, 502–505.
71. Bas, O.; Catelas, I.; De-Juan-Pardo, E.; Huttmacher, D.W. The quest for mechanically and biologically functional soft biomaterials via soft network composites. *Adv. Drug Deliv. Rev.* **2018**, *132*, 214–234. [CrossRef]
72. Schuurman, W.; Levett, P.A.; Pot, M.W.; van Weeren, P.R.; Dhert, W.J.A.; Huttmacher, D.W.; Melchels, F.P.W.; Klein, T.J.; Malda, J. Gelatin-Methacrylamide Hydrogels as Potential Biomaterials for Fabrication of Tissue-Engineered Cartilage Constructs. *Macromol. Biosci.* **2013**, *13*, 551–561. [CrossRef]
73. Berczyński, P.; Kładna, A.; Kruk, I.; Aboul-Enein, H.Y. Radical-scavenging activity of penicillin G, ampicillin, oxacillin, and dicloxacillin. *Luminescence* **2017**, *32*, 434–442. [CrossRef]
74. Klotz, B.J.; Gawlitta, D.; Rosenberg, A.J.; Malda, J.; Melchels, F.P. Gelatin-Methacryloyl Hydrogels: Towards Biofabrication-Based Tissue Repair. *Trends Biotechnol.* **2016**, *34*, 394–407. [CrossRef]
75. Andrzejewska, E. Photopolymerization kinetics of multifunctional monomers. *Prog. Polym. Sci.* **2001**, *26*, 605–665. [CrossRef]
76. Liu, M.; Li, M.-D.; Xue, J.; Phillips, D.L. Time-Resolved Spectroscopic and Density Functional Theory Study of the Photochemistry of Irgacure-2959 in an Aqueous Solution. *J. Phys. Chem. A* **2014**, *118*, 8701–8707. [CrossRef] [PubMed]
77. O’Connell, C.D.; Zhang, B.; Onofriello, C.; Duchi, S.; Blanchard, R.; Quigley, A.; Bourke, J.; Gambhir, S.; Kapsa, R.; Di Bella, C.; et al. Tailoring the mechanical properties of gelatin methacryloyl hydrogels through manipulation of the photocrosslinking conditions. *Soft Matter* **2018**, *14*, 2142–2151. [CrossRef] [PubMed]
78. Odian, G. *Principles of polymerization*, 4th ed.; John Wiley & Sons, Inc.: Hoboken, NJ, USA, 2004.
79. Pedroso, T.M.; Salgado, H.R.N. Validation of Cefazolin Sodium by UV-Spectrophotometric Method. *Phys. Chem.* **2013**, *3*, 11–20. [CrossRef]
80. Visscher, L.E.; Dang, H.P.; Knackstedt, M.A.; Huttmacher, D.W.; Tran, P.A. 3D printed Polycaprolactone scaffolds with dual macro-microporosity for applications in local delivery of antibiotics. *Mater. Sci. Eng. C* **2018**, *87*, 78–89. [CrossRef]
81. Rotilie, C.A.; Fass, R.J.; Prior, R.B.; Perkins, R.L. Microdilution Technique for Antimicrobial Susceptibility Testing of Anaerobic Bacteria. *Antimicrob. Agents Chemother.* **1975**, *7*, 311–315. [CrossRef]

82. Mohammed, I.; Said, D.G.; Nubile, M.; Mastropasqua, L.; Dua, H.S. Cathelicidin-Derived Synthetic Peptide Improves Therapeutic Potential of Vancomycin Against *Pseudomonas aeruginosa*. *Front. Microbiol.* **2019**, *10*, 2190. [[CrossRef](#)]
83. Vigata, M.; Meinert, C.; Hutmacher, D.W.; Bock, N. Hydrogels as Drug Delivery Systems: A Review of Current Characterization and Evaluation Techniques. *Pharmaceutics* **2020**, *12*, 1188. [[CrossRef](#)]
84. Kelm, J.; Regitz, T.; Schmitt, E.; Jung, W.; Anagnostakos, K. In Vivo and In Vitro Studies of Antibiotic Release from and Bacterial Growth Inhibition by Antibiotic-Impregnated Polymethylmethacrylate Hip Spacers. *Antimicrob. Agents Chemother.* **2006**, *50*, 332–335. [[CrossRef](#)]
85. Welch, A.B. Antibiotics in acrylic bone cement. In vivo studies. *J. Biomed. Mater. Res.* **1978**, *12*, 843–855. [[CrossRef](#)]
86. Seldes, R.M.; Winiarsky, R.; Jordan, L.C.; Baldini, T.; Brause, B.; Zodda, F.; Sculco, T.P. Liquid Gentamicin in Bone Cement. *J. Bone Jt. Surg.-Am. Vol.* **2005**, *87*, 268–272. [[CrossRef](#)]